Available online at www.sciencedirect.com
ScienceDirect
European Journal of Pharmaceutics and Biopharmaceutics 65 (2007) 215–232
European Journal of Pharmaceutics and Biopharmaceutics
www.elsevier.com/locate/ejpb

Research paper

Reversed chitosan–alginate polyelectrolyte complex for stability improvement of alpha-amylase: Optimization and physicochemical characterization

Mayur G. Sankalia *, Rajashree C. Mashru, Jolly M. Sankalia, Vijay B. Sutariya

Center of Relevance and Excellence in Novel Drug Delivery Systems, Pharmacy Department, The M. S. University of Baroda, Vadodara, India

Received 10 April 2006; accepted in revised form 4 July 2006
Available online 12 August 2006

Abstract

The present work explores, using response surface methodology, the main and interaction effects of some process variables on the preparation of a reversed chitosan–alginate polyelectrolyte complex (PEC) with entrapped α-amylase for stability improvement. A 3^3 full factorial design was used to investigate the effect of the chitosan and alginate concentrations and hardening time on the percent entrapment, time required for 50% (T_{50}) and 90% (T_{90}) enzyme release, and particle size. The beads were prepared by dropping chitosan containing α-amylase into a sodium alginate solution without any salt. The in vitro enzyme release profile of the beads was fitted to various release kinetics models to study the release mechanism. A topographical characterization was carried out using scanning electron microscopy (SEM), and the entrapment was confirmed using Fourier transform infrared (FTIR) spectroscopy and differential scanning calorimetry (DSC). Stability testing was carried out according to the International Conference on Harmonization (ICH) guidelines for zones III and IV. Beads prepared using 2.5% w/v chitosan and 3% w/v sodium alginate with a hardening time of 60 min had more than 90% entrapment and a T_{90} value greater than 48 min. Moreover, the shelf-life of the enzyme-loaded beads was found to increase to 3.68 years, compared with 0.99 years for the conventional formulation. It can be inferred that the proposed methodology can be used to prepare a reversed PEC of chitosan and alginate with good mechanical strength, provided both the reactants are in a completely ionized form at the time of the reaction. Proper selection of the reaction pH, polymer concentration and hence charge density, and hardening time is important and determines the characteristics of the PEC.
© 2006 Elsevier B.V. All rights reserved.

Keywords: Alginate; α-Amylase; Chitosan; In vitro release models; Polyelectrolyte complex (PEC); Stability

1. Introduction

α-Amylase, a major enzyme used for replacement of pancreatic enzymes [1], is not reabsorbed in the intestine like other proteins used for systemic therapy. Fungal α-amylases (EC 3.2.1.1; CAS 9000-90-2) are obtained from various strains of *Aspergillus* species (mainly *A. niger*, *A. awamori*, and *A. usamii*). α-Amylases catalyze the hydrolysis of α-1,4 glycosidic linkages in starch and other related carbohydrates. The active site has a large number of charged groups, among which are three acids (Asp231, Glu261, and Asp328, numbered according to the BLA sequence) essential to catalytic activity. α-Amylases are used in several industrial processes such as starch liquefaction, laundering, dye removal, and feed preprocessing, but the largest volume is sold to the starch industry for the production of high-fructose syrups and ethanol [2].

Pharmaceutical formulations containing α-amylase and other digestive enzymes need to be stored under cold (2–8 °C) or cool (8–25 °C) conditions and have a shelf-life

* Corresponding author. Center of Relevance and Excellence in Novel Drug Delivery Systems, Pharmacy Department, G.H. Patel Building, Donor's Plaza, The M. S. University of Baroda, Vadodara 390 002, India. Tel.: +91 265 2434187/2794051; fax: +91 265 2418927.
E-mail addresses: sankalia_mayur@hotmail.com (M.G. Sankalia), rajshreemashru@yahoo.com (R.C. Mashru), jollymayur@hotmail.com (J.M. Sankalia).

0939-6411/$ - see front matter © 2006 Elsevier B.V. All rights reserved.
doi:10.1016/j.ejpb.2006.07.014

of up to 1 year. Entrapment of the α-amylase in a biodegradable polyelectrolyte complex (PEC) may improve the stability of the parent enzyme [3,4] and make it less prone to interference from the various excipients of the formulation. Immobilized enzymes are stable at higher temperatures and may be stored at room temperature with an extended shelf-life [5]. These advantages are of great interest from a commercial viewpoint for the pharmaceutical industry. Hence, it was the objective of this research to develop an extended shelf-life formulation of α-amylase by entrapping it in biodegradable chitosan–alginate PEC beads, with a resultant improved and efficient utilization of the enzyme. This paper also deals with in vitro dissolution studies and physicochemical characterization carried out to evaluate the beads and their release behavior.

Chitin (β(1–4)-*N*-acetyl-D-glucosamine), the second most abundant naturally occurring biopolymer after cellulose, is the major structural component of the invertebrate exoskeleton and the fungal cell wall [6]. Waste produced in the processing of seafood, mainly crab, shellfish, lobster, and shrimp, is an abundant source of chitin. Chitosan, obtained by partial alkaline deacetylation of chitin, is a polycationic polysaccharide consisting of β-[1 → 4]-linked 2-acetamido-2-deoxy-β-D-glucopyranose (GlcNAc; A-unit) and 2-amino-2-deoxy-β-D-glucopyranose (GlcN; D-unit) (Fig. 1A) [7] and has a macro pK_a value in the range of 6.3–6.5. Chitosan and chitin are commercially interesting compounds because of their high nitrogen content (6.89%; the repeating unit contains the $-NH_2$ group at the C-2 position) [8] compared with synthetically substituted cellulose (1.25%). This makes chitosan a useful chelating agent [9]. This polysaccharide becomes water-soluble under acidic conditions (pH < 6), allowing the preparation of biocompatible and often biodegradable polymer solutions [10]. Also, it has excellent cell-adhesive properties [11], promotes wound–healing [12], and has bacteriostatic effects [13]. Moreover, chitosan is metabolized by certain human enzymes, e.g., lysozyme [14], α-amylase [14], and hyaluronidase, and can be considered biodegradable [14]. Finally, chitosan is abundant in nature, and it is cheap to produce, apart from being ecologically interesting [15].

Alginate, a high-molecular-mass hyaluronic acid-like biodegradable polymer, is a naturally occurring copolymer of 1,4-linked β-D-mannuronic acid (M) and α-L-guluronic acid (G) (Fig. 1B) extracted from brown seaweeds (Phaeophyceae, mainly *Laminaria*). The pK_a values of

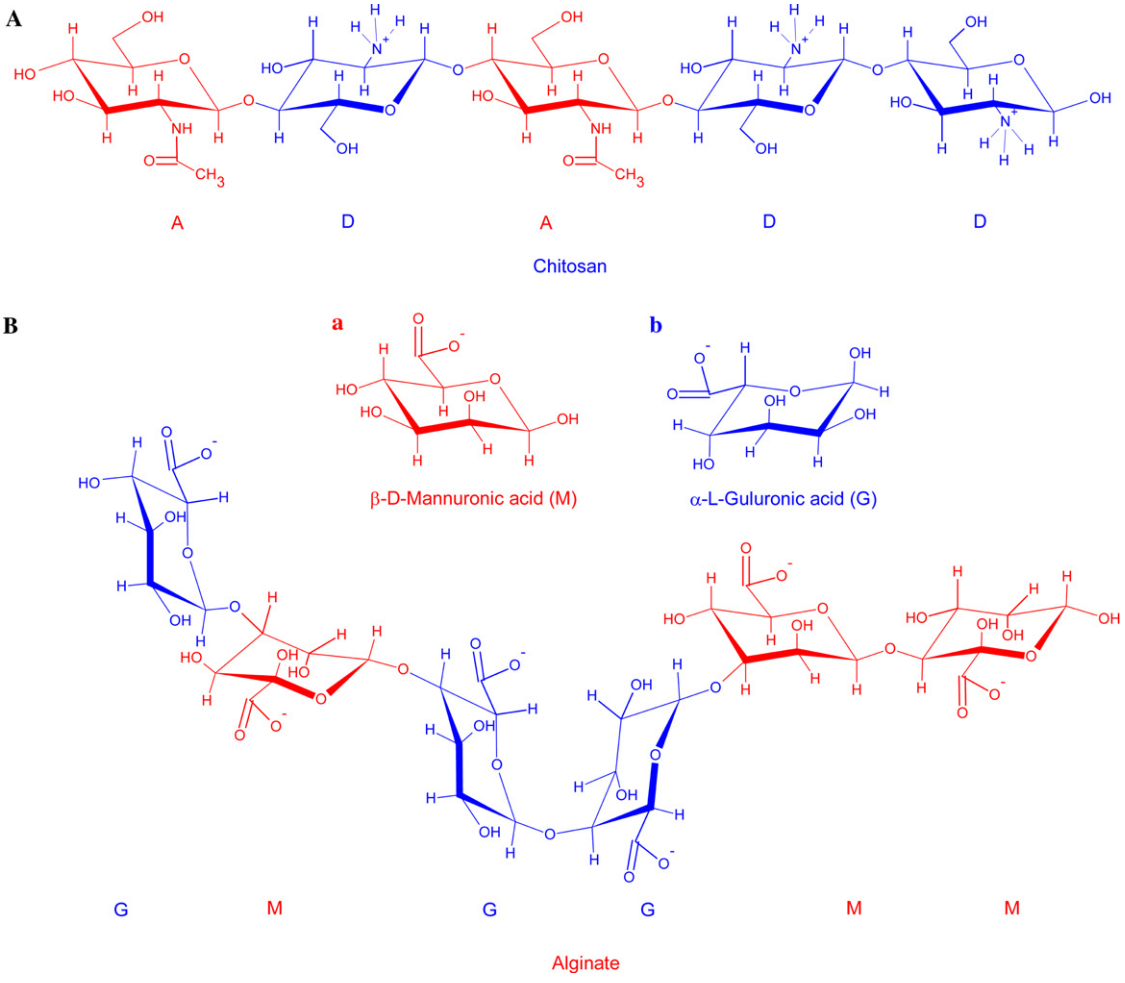

Fig. 1. Chemical structures of (A) chitosan and (B) alginate.

M- and G- residues are 3.38 and 3.65, respectively. By virtue of the carboxyl groups on the constituent uronic acid residues, the pK_a value of alginic acid ranges between 3.4 and 4.4, depending on the type of alginate and the salts present in the mixture [16]. It has been shown that the G and M units are joined together in blocks, and as such, three types of block may be found: homopolymeric G blocks (GG), homopolymeric M blocks (MM), and heteropolymeric sequentially alternating blocks (MG). Alginate is chemically very stable at pH values between 5 and 10. High acid concentrations cause decarboxylation of alginate [17]. Alginate beads have the advantages of being non-toxic orally and having high biocompatibility [18]. Alginate is used as an entrapment matrix for cells and enzymes and as a pharmaceutical and food adjuvant.

The formation of polyanion–polycation (polyelectrolyte) complexes is mainly driven by an electrostatic mechanism where charge neutralization and possible local overcompensation or bridging (such as hydrogen bonding, Coulomb forces, van der Waals forces, and transfer forces) mediated by a multivalent counterion induces attraction between topologically separated segments of the polyelectrolytes [3]. The lower the charge density of the polymer, the higher is the polymer proportion in the PEC, since more polymeric chains are required to react with the other polymer, leading to 'bulky' PEC [19]. Since chitosan has a rigid, stereo-regular structure containing bulky pyranose rings, the formation of PEC can induce a conformational change of the other polyelectrolyte if the latter has a non-rigid structure [20]. PECs of different characteristics can be obtained by changing the chemical characteristics of the component polymers, such as the molecular weight, flexibility, functional group structure, charge density, hydrophilicity and hydrophobicity balance, and stereo-regularity and compatibility, as well as the reaction conditions: the pH, ionic strength, concentration, mixing ratio, and temperature [3].

Beads produced from sodium alginate with calcium chloride present in the chitosan solution bind ~100 times more chitosan than do capsules produced by dropping the alginate solution in a chitosan solution in the absence of salt, and most beads, micro- and macrocapsules, and microspheres are produced by these methods. Reversed chitosan–alginate complex coacervate capsules, formed by dropwise addition of chitosan solution into alginate solution, were reported to be fragile even after hardening for 3 h [21]. To avoid the limitation of this reverse coacervation, the present study employs a novel approach, wherein chitosan and alginate are reacted in their completely ionized states to increase the counterion charge density of the polymers, which increases the overall interaction and hence the mechanical strength of the PEC membrane. This was achieved by maintaining the pH values of the chitosan and alginate solutions at 2 and 6.5, respectively. Further, the pH value of 2 of the chitosan solution suppresses the chitolytic activity of the added α-amylase, which is active in a pH range of 4–5.

2. Materials and methods

2.1. Materials

Potassium dihydrogen phosphate, sodium hydroxide (NaOH), hydrochloric acid (HCl) (Qualigens Fine Chemicals, Mumbai, India), and soluble starch (Himedia Laboratories Pvt. Ltd., Mumbai, India) were used as received. Fungal α-amylase, sodium alginate, iodine, and potassium iodide were purchased from S. D. Fine-Chem Ltd., Mumbai, India. Chitosan (Chito Clear®) with a reported degree of deacetylation of 89% (titration method) was a kind gift from Primex ehf, Ireland. The average molecular weight of the chitosan was determined through gel permeation chromatography (GPC) and was found to be ≈285 kDa. All the other chemicals and solvents were of analytical grade and were used without further purification. Deionized double-distilled water was used throughout the study.

2.2. Preparation of chitosan–alginate PEC beads

Chitosan–alginate PEC beads were produced from a pair of oppositely charged polysaccharides. A 1–3% w/v aqueous sodium alginate solution was prepared in deionized double-distilled water. The pH value of the solution was 6.13 ± 0.2 and was adjusted to 6.5 ± 0.1 using 0.1 N NaOH. An aqueous chitosan solution was prepared by dissolving an appropriate quantity of chitosan powder in 30 ml of 0.1 M HCl. The required quantity of enzyme (200 mg α-amylase in 50 ml of final chitosan solution) was dissolved in a small quantity of water and mixed with concentrated chitosan solution. The final concentration of the chitosan solution was adjusted to be in the range of 1.5–2.5% w/v and was used after degassing under a vacuum. Approximately 10 ml of enzyme-containing chitosan was introduced into a 10-ml glass syringe with an 18 G × 1/2″ flat-cut hypodermic needle. There was a slight drop in the pH value after the addition of the chitosan solution because of its acidic pH and because there was no buffer system added to the sodium alginate solution. The final reaction pH value was around 6.5 ± 1.0. The droplets were sheared off for 120 s at a flow rate of 5 ml/min into 50 ml of sodium alginate solution. The resulting beads were allowed to harden for 30–60 min under gentle stirring (100 rpm) with a small magnetic bar, decanted on a Buchner funnel, rinsed with deionized double-distilled water, and dried to a constant weight in a vacuum desiccator (Tarsons Products Pvt. Ltd., Kolkata, India) at room temperature over 48 h. The entire capsule formation procedure described herein was carried out at ambient temperature. The different values of the independent variables (chitosan and sodium alginate concentrations and hardening time) and the dependent variables (percent entrapment, T_{50}, T_{90}, and particle size) with constraint used in the study are listed in Table 1. The PEC membrane formation may be schematically classified into three main stages: (i) primary complex formation; (ii) formation process within

Table 1
Process variables and responses with constraints for 3^3 full factorial design

Factors	Coded levels	Actual levels
A: Chitosan concentration (% w/v)	−1	1.5
	0	2.0
	1	2.5
B: Sodium alginate concentration (% w/v)	−1	1
	0	2
	1	3
C: Hardening time (min)	−1	30
	0	45
	1	60
Responses	Constraint	
M_1: % Entrapment	>90%	
M_2: T_{50} (min)	–	
M_3: T_{90} (min)	>48 min	
M_4: Particle size (mm)	–	

intracomplexes; and (iii) intercomplex aggregations. Prior mixing results in a randomly arranged primary complex (due to secondary binding sources such as Coulomb forces, very rapid), which upon further exposure is converted to an ordered secondary complex (due to the formation of new bonds and/or the straightening of the distortions of the polymer chain) and contains water molecules [22]. Upon drying, the PEC membrane undergoes intercomplex aggregation (because of hydrophobic interactions and/or drying), creating a network [23].

2.3. 3^3 Full factorial design (FFD)

Statistical experimental designs have been in use for several decades [24,25]. These experimental layouts can be adopted at various phases of an optimization process, such as in screening experiments or in finding the optimal conditions for targeted results. The results of a statistically planned experiment are better accepted than those of traditional single-variable experiments. Response surface methodology is now established as a convenient method for developing optimum processes with precise conditions and has minimized the cost of production of many a process with efficient screening of process parameters.

In order to attain the maximum entrapment and an extended T_{90}, a three-level FFD was employed (number of runs $N = 3^f$, where f is the number of independent variables). Before application of the design, a number of preliminary trials were conducted to determine the conditions under which the process produced beads. To determine the experimental error, the experiment at the center point was repeated three times on different days. The mean percent entrapment, T_{50}, T_{90}, and particle size at the center-replicated points were $86.31 \pm 0.24\%$, 37.06 ± 0.37 min, 43.09 ± 0.39 min, and 1.43 ± 1.07 mm, respectively, indicating the reproducibility of the process was good. For predicting the optimal region, a second-order polynomial function was fitted to correlate the relationship between the variables and the responses. The behavior of the system was explained using the following quadratic equation:

$$Y = \beta_0 + \sum \beta_i x_i + \sum \beta_{ij} x_i x_j + \sum \beta_{ii} x_i^2 \quad (1)$$

where Y is the predicted response, β_0 is the offset term (model constant), β_i is the linear offset, β_{ii} is the squared offset, β_{ij} is the interaction effect, and x_i is the dimensionless coded value of the independent variable (X_i). From the quadratic equation, response surfaces were generated, and the overlapping region of the responses with constraint was identified as the optimum region where the beads matching the desired criteria could be produced. Analysis of variance (ANOVA) was carried out to determine the significance of the fitted equation. All analytical treatments were performed using NCSS software. The quality of fit of the polynomial model equation was expressed by the adjusted coefficient of determination, R^2_{adj}. All experimental designs were randomized to exclude any bias. The process variables, their coded experimental values, and the responses are listed in Table 2.

2.4. Curve fitting

The in vitro release pattern was evaluated to check the goodness of fit to the zero-order release kinetics (Eq. (2)), first-order release kinetics [26,27] (Eq. (3)), Higuchi's square root of time equation [28] (Eq. (4)), Korsmeyer–Peppas' power law equation [29,30] (Eq. (5)), and Hixson–Crowell's cube root of time equation [31] (Eq. (6)). The goodness of fit was evaluated using the r (correlation coefficient) values. To obtain a better understanding, residual analysis [32] of the above models was performed on the optimized formulation.

$$Q_t = Q_0 + K_0 t \quad (2)$$

where Q_t is the amount of drug dissolved in time t, Q_0 is the initial amount of drug in the solution (usually $Q_0 = 0$), K_0 is the zero-order release constant, and t is the release time.

$$Q_t = Q_0 e^{-K_1 t} \quad (3)$$

where Q_t is the amount of drug dissolved in time t, Q_0 is the initial amount of drug in the solution, K_1 is the first-order release constant, and t is the release time.

$$Q_t = K_H \sqrt{t} \quad (4)$$

where Q_t is the amount of drug dissolved in time t, K_H is the Higuchi dissolution constant, and t is the release time.

$$Q_t/Q_\infty = K_k t^n \quad (5)$$

where Q_t is the amount of drug dissolved in time t, Q_∞ is the amount of drug dissolved after infinite time (all the drug loaded in the formulation), Q_t/Q_∞ is the fractional release of the drug in time t, K_k is a constant incorporating the structural and geometric characteristics of the dosage form, n is the release (diffusional) exponent, which depends on the release mechanism and the shape of the matrix test-

Table 2
Matrix of 3^3 full factorial design and results for the measured responses

ES[a]	Factors/levels			Responses			
	Chitosan (% w/v)	Sodium alginate (% w/v)	Hardening time (min)	% Immobilization[b]	T_{50}[b,c]	T_{90}[b,c]	Particle size[d] (mm)
19	−1	−1	−1	82.21 ± 0.11	29.20 ± 0.15	33.50 ± 0.15	1.02 ± 0.03
11	−1	−1	0	81.48 ± 0.09	33.30 ± 0.16	38.40 ± 0.15	1.01 ± 0.04
24	−1	−1	1	81.18 ± 0.12	36.40 ± 0.19	43.70 ± 0.21	1.01 ± 0.04
31	−1	0	−1	85.22 ± 0.11	34.70 ± 0.14	40.50 ± 0.19	0.96 ± 0.05
23	−1	0	0	84.57 ± 0.09	38.80 ± 0.24	44.60 ± 0.24	0.95 ± 0.05
20	−1	0	1	84.26 ± 0.11	42.40 ± 0.18	49.20 ± 0.23	0.95 ± 0.04
7	−1	1	−1	88.55 ± 0.10	40.50 ± 0.20	46.50 ± 0.20	0.91 ± 0.05
16	−1	1	0	87.97 ± 0.11	44.05 ± 0.19	51.60 ± 0.29	0.91 ± 0.04
4	−1	1	1	87.61 ± 0.13	48.10 ± 0.19	55.60 ± 0.20	0.91 ± 0.05
29	0	−1	−1	83.66 ± 0.10	27.20 ± 0.16	33.50 ± 0.15	1.53 ± 0.05
5	0	−1	0	83.00 ± 0.09	31.50 ± 0.17	38.55 ± 0.12	1.52 ± 0.03
17	0	−1	1	82.71 ± 0.12	34.40 ± 0.12	40.40 ± 0.27	1.52 ± 0.05
25	0	0	−1	86.85 ± 0.12	33.30 ± 0.12	38.30 ± 0.17	1.44 ± 0.02
21	0	0	0	85.99 ± 0.13	37.06 ± 0.24	43.61 ± 0.25	1.44 ± 0.04
22	0	0	0	86.28 ± 0.12	36.84 ± 0.22	42.53 ± 0.20	1.43 ± 0.05
10	0	0	0	86.27 ± 0.10	37.00 ± 0.19	43.20 ± 0.20	1.43 ± 0.05
26	0	0	0	86.65 ± 0.13	37.68 ± 0.20	43.19 ± 0.19	1.44 ± 0.04
18	0	0	0	86.37 ± 0.12	36.74 ± 0.20	42.94 ± 0.29	1.43 ± 0.03
6	0	0	1	85.94 ± 0.11	40.15 ± 0.21	47.20 ± 0.25	1.43 ± 0.03
13	0	1	−1	90.38 ± 0.12	38.70 ± 0.21	44.20 ± 0.32	1.38 ± 0.04
27	0	1	0	89.88 ± 0.13	43.20 ± 0.22	49.50 ± 0.30	1.37 ± 0.03
1	0	1	1	89.51 ± 0.11	46.55 ± 0.20	52.95 ± 0.31	1.37 ± 0.04
15	1	−1	−1	85.35 ± 0.11	26.30 ± 0.17	31.30 ± 0.15	1.94 ± 0.03
3	1	−1	0	84.74 ± 0.13	30.30 ± 0.12	36.10 ± 0.13	1.94 ± 0.06
2	1	−1	1	84.46 ± 0.13	33.05 ± 0.16	38.50 ± 0.14	1.93 ± 0.06
9	1	0	−1	88.93 ± 0.11	31.80 ± 0.14	37.30 ± 0.14	1.81 ± 0.04
30	1	0	0	88.42 ± 0.13	35.40 ± 0.17	41.50 ± 0.27	1.80 ± 0.05
14	1	0	1	88.11 ± 0.09	38.80 ± 0.17	44.30 ± 0.25	1.80 ± 0.05
28	1	1	−1	92.64 ± 0.09	37.20 ± 0.20	42.85 ± 0.27	1.73 ± 0.03
8	1	1	0	92.24 ± 0.11	40.40 ± 0.22	46.80 ± 0.24	1.72 ± 0.04
12	**1**	**1**	**1**	**91.91 ± 0.13**	**44.15 ± 0.21**	**49.90 ± 0.30**	**1.72 ± 0.04**

[a] ES, experimental sequence.
[b] $n = 3$.
[c] T_{50} and T_{90} were determined from release profile in SGF without enzyme pH 1.2 (USP XXVI) at 37 ± 0.5 °C.
[d] $n = 50$.

ed [33], and t is the release time. An interpretation of the diffusional exponent is given in Table 3.

$$Q_0^{1/3} - Q_t^{1/3} = K_s t \quad (6)$$

where Q_0 is the initial amount of drug in the pharmaceutical dosage form, Q_t is the remaining amount of drug in the pharmaceutical dosage form at time t, K_s is a constant incorporating the surface–volume relation, and t is the release time.

In order to understand the release mechanism, the release data of the optimized batch were fitted to an empirical equation proposed by Kopcha [34] (Eq. (7)),

Table 3
Interpretation of Korsmeyer-Peppas power law release exponent

Release exponent (n)	Drug transport mechanism	Rate as a function of time
0.5	Fickian diffusion	$t^{-0.5}$
$0.5 < n < 1.0$	Anomalous transport	t^{n-1}
1.0	Case-II transport	Zero order release
Higher than 1.0	Super Case-II transport	t^{n-1}

$$M = At^{1/2} + Bt \quad (7)$$

In this equation (Eq. (7)), M (⩽70%) is the percentage of drug released at time t, while A and B are, respectively, the diffusion and erosion terms. According to this equation, if the diffusion to erosion ratio $A/B = 1$, then the release mechanism involves diffusion and erosion equally. If $A/B > 1$, then diffusion prevails, while erosion predominates when $A/B < 1$.

2.5. Characterization of beads

2.5.1. Estimation of α-amylase (dextrinogenic assay)

The iodine test of Smith and Roe [35,36] was modified as follows: Two milliliters of a 0.2% starch solution was added to 1.0 ml of enzyme diluted in 0.05 M phosphate buffer of pH 6.8. The mixture was incubated for 3 min at 25 °C, and then the reaction was stopped with 1 ml of 1 N HCl. Finally, 20 ml of water and 0.5 ml of 0.01 N iodine solution prepared according to Rice [37] were added and the absorbance, A, was recorded using a spectrophotometer

(Shimadzu UV-1601, Japan) at 660 nm. The zero reading of the instrument was set using an iodine blank containing no enzyme or substrate. The dextrinogenic activity is expressed in arbitrary units as follows:

$$D = [(A_B - A)/A_B] \cdot E \quad (8)$$

where A_B is the absorbance of the starch–iodine complex in the absence of enzyme and E is the enzyme dilution. The best results were obtained when the enzyme solution was diluted so as to make the ratio $(A_B - A)/A_B$ approach 0.20–0.25.

2.5.2. Determination of entrapment efficiency

The entrapment efficiency was determined by dissolving the enzyme-loaded beads in a magnetically stirred simulated gastric fluid (SGF) without enzyme (USP XXVI) for about 90 min. The resulting solution was centrifuged at 2500 rpm for 10 min (Remi Instruments Ltd., Mumbai, India), and aliquots from the supernatant were adjusted to pH 6.8 using 0.01 M NaOH and diluted appropriately with 0.05 M phosphate buffer of pH 6.8 and assayed ($n = 3$) for enzyme content using the dextrinogenic method. The entrapment efficiency was calculated as

$$\text{Entrapment efficiency} = \frac{\text{Enzyme loaded}}{\text{Theoretical enzyme loading}} \times 100 \quad (9)$$

2.5.3. Determination of T_{50} and T_{90}

The durations required for 50% (T_{50}) and 90% (T_{90}) enzyme release were used to evaluate the onset and duration of action, respectively. For optimization purposes, the dissolution studies of all the batches were carried out in 500 ml of SGF without enzyme using the USP XXVI dissolution apparatus 2 (TDT-60 T, Electrolab, Mumbai, India) at 37 ± 0.5 °C with a paddle speed of 75 rpm. Accurately weighed samples ($n = 3$) equivalent to about 40 mg of α-amylase were subjected to dissolution, and aliquots of 2 ml were collected and assayed at 0, 5, 10, 15, 20, 25, 30, 35, 40, 45, 50, 55, 60, and 65 min. The T_{50} and T_{90} values were found by extrapolating the plot of the percent enzyme released versus time.

2.5.4. Particle size measurements

The particle sizes of 50 gel beads were measured using a gauge-type micrometer (0.01 mm least count, Durga Scientific Pvt. Ltd., Vadodara, India) for each formulation, and the mean particle size was determined.

2.5.5. Effect of pH on release profile

To study the effect of the pH value on the profile of the α-amylase release from the PEC, an in vitro dissolution study was carried out as before using 500 ml of media of different pH values (SGF without enzyme of pH 1.2, phosphate buffer of pH 4.0, simulated intestinal fluid (SIF) without enzyme of pH 6.8, and phosphate buffer of pH 7.4) on the optimized batch. Accurately weighed samples ($n = 3$) equivalent to about 40 mg of α-amylase were introduced into the dissolution media, and 2-ml samples were collected at 0, 0.25, 0.50, 0.75, 1.0, 1.5, 2.0, 2.5, 3.0, 3.5, 4.0, 4.5, 5.0, 5.5, and 6.0 h. The samples were filtered through Whatman® filter paper #42 and assayed for enzyme content as before.

2.5.6. Fourier transform infrared (FTIR) spectroscopy

Infrared transmission spectra were obtained using a FTIR spectrophotometer (FTIR-8300, Shimadzu, Japan). Two percent (w/w) of the sample, with respect to a potassium bromide (KBr; S. D. Fine Chem Ltd., Mumbai, India) disk, was mixed with dry KBr. The mixture was ground into a fine powder using an agate mortar and then compressed into KBr disks in a hydraulic press at a pressure of 10,000 psi. Each KBr disk was scanned 16 times at 4 mm/s at a resolution of 2 cm^{-1} over the wavenumber range of 400–4000 cm^{-1} using Happ–Genzel apodization. The characteristic peaks were recorded.

2.5.7. Differential scanning calorimetry (DSC)

Differential scanning calorimetric analysis was used to characterize the thermal behavior of the isolated substances, empty beads, and enzyme-loaded beads. DSC thermograms were obtained using an automatic thermal analyzer system (DSC-60, Shimadzu, Japan). Temperature calibration was performed using indium as the standard. Samples were crimped in a standard aluminum pan and heated from 40 to 400 °C at a heating rate of 10 °C/min under constant purging of dry nitrogen at 30 ml/min. An empty pan, sealed in the same manner as the samples, was used as a reference.

2.5.8. Scanning electron microscopy (SEM)

The purpose of the SEM study was to obtain a topographical characterization of the beads. The beads were mounted on brass stubs using carbon paste. SEM photographs were taken using a scanning electron microscope (JSM-5610LV; Jeol Ltd., Tokyo, Japan) at the required magnification at room temperature. A working distance of 39 mm was maintained, and the acceleration voltage used was 20 kV, with the secondary electron image (SEI) as the detector.

2.6. Preparation of capsule formulation, packaging, and stability study

Accurately weighed chitosan–alginate beads equivalent to 40 mg of α-amylase were filled into a hard gelatin capsule manually. The joint of the capsule body and cap was carefully sealed by pressing them so that they fitted in the lock mechanism. The capsules were packed in high-density polyethylene (HDPE) bottles with polypropylene (PP) caps (foamed polyethylene and pressure-sensitive liner). The capsules were subjected to stability testing according to the International Conference on Harmonization (ICH)

guidelines for zones III and IV. The packed containers of prepared capsules, the marketed formulation, and bulk α-amylase were subjected to accelerated (40 ± 2 °C/75 ± 5% relative humidity) and long-term (30 ± 2 °C/65 ± 5% relative humidity) stability tests for up to 12 months. For accelerated and long-term stability, desiccators containing saturated sodium chloride and potassium iodide solutions were kept in ovens at 40 and 30 °C to maintain a constant relative humidity of 74.68 ± 0.13 and 67.98 ± 0.23%, respectively. A visual inspection (for discoloration of capsule content), dissolution testing, and α-amylase content estimation were carried out every 15 days for the entire period of the stability study.

3. Results and discussion

3.1. Principle of PEC formation

The electrostatic attraction between the cationic amino groups of chitosan (the macro pK_a value is about 6.5) [38] and the anionic carboxyl groups of the alginate is the main interaction leading to the formation of the PEC. It is stronger than most secondary binding interactions [38]. For preparation of beads with reverse engineering, the formation of a membrane of good mechanical strength (precipitate) at the interface of the polymers is essential. This is required to avoid homogeneous mixing of the chitosan and alginate solutions and to maintain the geometry of the bead, which may otherwise be easily distorted even under the mild shear stress of the stirring. Table 4 indicates the effect of the pH values of the chitosan and alginate solutions on the properties of the beads. As can be seen, condition M-2 resulted in spherical beads with no aggregates. Moreover, the membrane was thin, but the mechanical strength was good. With an acidic environment, the chitosan is highly protonated, and in a neutral or alkaline environment, the alginate is decidedly anionic. The maximum interaction between the amino and carboxyl groups takes place under condition M-2 and results in a compact membrane. Moreover, the chitolytic activity of the α-amylase can be suppressed almost entirely in an acidic chitosan solution (α-amylase is functionally inactive at acidic pH values) to prevent the digestion of chitosan.

3.2. Effect of the factors on the responses

3.2.1. Percent entrapment

The ANOVA results and the regression coefficients of the response variables are shown in Table 5. All three process variables were statistically significant ($P < 0.05$). From the contour plots of the response surface for percent entrapment (Fig. 2) and Table 5, it can be concluded that the concentration of alginate was the factor with the greatest influence and had a positive effect (i.e., response increases with increase in factor level). However, the hardening time affected negatively (i.e., response decreases with increase in factor level) significantly. More than 90% entrapment (experiments 28, 8, and 12) was obtained at the higher value of all three process variables.

On addition of a chitosan solution to alginate solution, instantaneous interfacial cross-linking takes place, the speed being proportional to the charge density of the solutions. A higher concentration of the polymers and pH values corresponding to their ionized state result in an increased charge density of both the polymers and will lead to intense cross-linking with small micropores. This might be the cause of the minimized loss of enzyme from the PEC beads and higher percent entrapment values at higher polymer concentrations. However, a longer hardening time may cause deeper penetration of the alginate into the chitosan solution, inactivate the greater part of the enzyme, and result in lower percent entrapment values.

3.2.2. T_{50} and T_{90}

As shown in Fig. 2 and Table 5, all three factors had significant positive effects on both response values. The alginate concentration (factor B) was found to be the factor with the greatest influence. For maximum activity of the enzyme in the intestine, higher T_{50} and T_{90} values were the desired criteria of the optimum formulation. Thus, the highest values of all three variables produced beads with T_{50} and T_{90} values as high as 44.15 and 49.9 min, respectively (experiment 12, Table 2). The T_{50} and T_{90} values were found to be proportional to the alginate concentration and hardening time, while they were inversely proportional to the chitosan concentration. This may explained as follows.

Table 4
Effect of chitosan and alginate solution pH on beads properties[a]

Sr. No.	pH		Mechanical strength of membrane[b]	Membrane thickness	Comments
	Chitosan solution	Alginate solution			
M-1	2	3.5	− + −	Thick	Alginate viscosity very high, bead shape distorted, beads aggregated
M-2	2	6.5	+ + +	Thin	Spherical beads, no aggregate
M-3	5.4	3.5	− − −	Very thin	Lump of chitosan after few minutes, chitosan and alginate viscosity very high
M-4	5.4	6.5	− + −	Thin	Chitosan viscosity very high, beads aggregated

[a] Results are comparative for 2% w/v chitosan, 2% w/v alginate, and 30 min hardening time.
[b] + + +, excellent; − + −, good; − −−, poor.

Table 5
ANOVA results (P values): effect of the variables on % entrapment, T_{50}, T_{90}, and particle size

Factors	% Entrapment		T_{50}[b]		T_{90}[b]		Particle size	
	Coefficient[a]	P	Coefficient[a]	P	Coefficient[a]	P	Coefficient[a]	P
Intercept	86.31	<0.0001*	37.08	<0.0001*	43.24	<0.0001*	1.43	<0.0001*
A	1.88	<0.0001*	−1.67	<0.0001*	−1.95	<0.0001*	0.43	<0.0001*
B	3.44	<0.0001*	5.62	<0.0001*	5.89	<0.0001*	−0.08	<0.0001*
C	−0.45	<0.0001*	3.62	<0.0001*	4.10	<0.0001*	0.00	0.0013*
A^2	0.19	0.0004*	0.05	0.7052	−0.11	0.5555	−0.05	<0.0001*
B^2	0.12	0.0102*	−0.01	0.9315	0.17	0.3772	0.02	<0.0001*
C^2	0.12	0.0101*	−0.28	0.0366*	−0.52	0.0119*	0.00	0.5583
AB	0.25	<0.0001*	−0.14	0.1623	−0.37	0.0182*	−0.03	<0.0001*
AC	0.04	0.2355	−0.15	0.1291	−0.56	0.0009*	0.00	0.8014
BC	0.03	0.4198	0.10	0.2847	0.05	0.7324	0.00	0.7243
ABC	0.01	0.8327	−0.02	0.8316	0.12	0.5091	0.00	0.4377
$r^2_{adj.}$	0.9986		0.9962		0.9926		0.9998	

[a] Regression coefficients are in coded values.
[b] T_{50} and T_{90} were determined from release profile in SGF without enzyme pH 1.2 (USP XXVI) at 37 ± 0.5 °C.
* Statistically significant ($P < 0.05$).

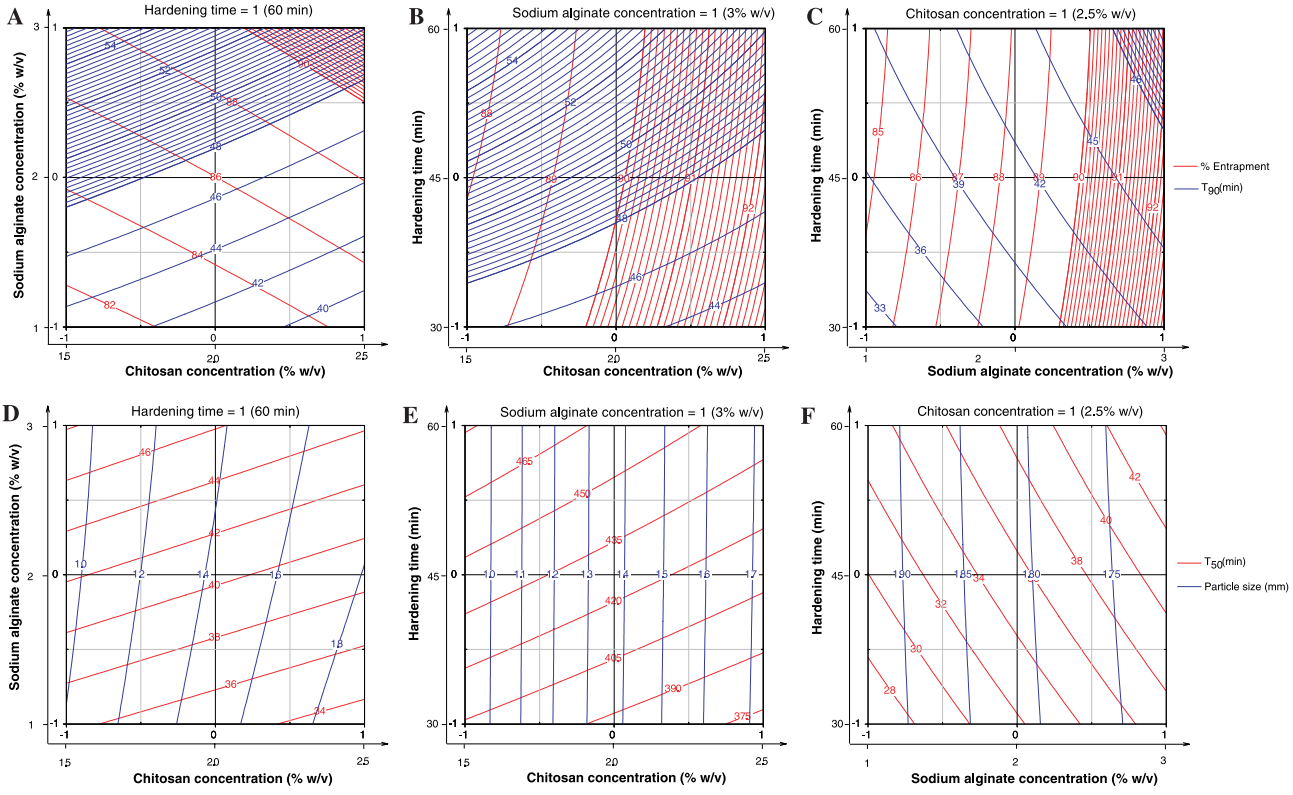

Fig. 2. Contour plots of % entrapment, T_{90}, T_{50}, and particle size as a function of chitosan concentration, sodium alginate concentration, and hardening time. T_{50} and T_{90} were determined from release profile in SGF without enzyme pH 1.2 (USP XXVI) at 37 ± 0.5 °C.

The alginate forms the outer layer of the beads. Thus a higher concentration of alginate provides higher charge density of the alginate carboxyl group and results in higher cross-linking of the PEC, and thus it produces a stronger PEC membrane with a lower thickness and small micropores. Similarly, a low alginate concentration provides a low charge density of –COO^-, and there is less cross-linking, resulting in a thick, weak PEC membrane with large micropores. Alginate, upon exposure to acidic dissolution media, might be converted to alginic acid, which is more viscous than alginate and causes delayed dissolution of the beads. Similarly, as mentioned in the foregoing, a longer hardening time may cause deeper penetration of the alginate into the chitosan and produce a thick PEC at the surface, which will require a longer time for complete dissolution. The release of enzyme from the beads is due to

bursting of the PEC membrane (see Section 3.6). In the core of the beads, the chitosan is not complexed with alginate and thus provides a good hypertonic environment for osmosis to occur. As the chitosan concentration increases, the hypertonicity also increases and exerts a greater osmotic pressure against the PEC membrane. Thus, a higher concentration of chitosan leads to an early bursting effect and low T_{50} and T_{90} values.

3.2.3. Particle size

As shown in Table 5, the chitosan concentration (factor A, most influential) had a positive coefficient, while the alginate concentration had a negative coefficient. All three process variables were statistically significant ($P < 0.05$). The bead size is influenced by the orifice of the needle through which the chitosan is allowed to pass, addition of surfactant, and extrusion rate (which were kept constant) and the surface tension and the viscosity of the chitosan solution. The increased viscosity at higher concentrations of chitosan resulted in larger particles. As before, a higher concentration of alginate gives rise to a higher charge density and results in stronger but thin membranes with small micropores. Thus, an increased alginate concentration causes a decrease in the particle size. In the same way, a low alginate concentration gives rise to a low charge density and results in a weak, 'bulky' membrane with an increased particle size. The hardening time does not affect the particle size (the coefficient is zero), and this indicates that the chitosan–alginate interaction is instantaneous and the membrane formed upon first exposure is hard enough to restrict the expansion or constriction caused by a longer hardening time.

3.3. Interactions between the factors

An interaction is the failure of a factor to produce the same effect on the response at different levels of another factor. The ANOVA results (Table 5) showed that the interaction AB had a significant influence on percent entrapment, T_{90}, and particle size, while the interaction AC had a significant effect on only T_{90}. However, other interaction terms were non-significant statistically. Analysis of the results by multiple regression (Table 5) yields equations that adequately describe the influence of the selected factors on percent entrapment, T_{50}, T_{90}, and particle size.

3.4. Optimization of the process using response surfaces

Generally, the aim of optimization is to find the optimum levels of the variables that affect a process, whereby a product of desired characteristics can be produced easily and reproducibly. Using the response surface of selected responses with constraint (percent entrapment >90% and $T_{90} > 48$ min), it was possible to identify the optimum region. The contour plots that describe the influence of the independent factors on the percent entrapment and T_{90} have been presented in Figs. 2A–C. A study of these plots shows that beads with the desired characteristics could be produced at the highest values (+1) of all three process variables. Experiment 12 was a batch with the same experimental conditions and fulfilled both the constraints favorable for beads preparation. Hence, this was considered the optimum batch.

3.5. Evaluation of model using cross-validation

In order to assess the reliability of the model, five experiments were conducted by varying the process variables at values other than those of the model. For each of these experiments, the responses were estimated using the derived quadratic polynomial equations and determined experimentally for comparison (Table 6). The percent relative error was calculated from the following equation:

$$\text{Percent relative error} = \left[\frac{\text{predicted value} - \text{experimental value}}{\text{predicted value}}\right] \quad (10)$$

It can be seen that in all cases there was a reasonable agreement between the predicted and the experimental values, since the value of the percent relative error found was low. For this reason, it can be concluded that the equations describe adequately the influence of the selected process variables on the responses under study.

3.6. Curve fitting and release mechanism

The in vitro dissolution profile of the optimized batch is shown in Fig. 3A. The values of the release exponent (n) and the kinetic constant (K) were derived using zero-order kinetics, first-order kinetics, Higuchi's square root of time equation, Korsmeyer–Peppas' power law equation, and Hixson–Crowell's cube root of time equation, and these are presented in Table 7. The enzyme release data show a good fit to the Korsmeyer–Peppas' power law release kinetics (Eq. (5)), which can be confirmed by comparing the values of the correlation coefficient (r) with those of the other models. The values of the Korsmeyer–Peppas' release exponent (n) determined for the various formulations studied ranged from 2.08 to 2.72, suggesting probable release by super case-II transport. According to Brazel and Peppas, super case-II transport is observed due to a large increase in osmotic pressure driving forces [39]. The K_k values ranged from 0.003 to 0.93, with a low K_k value suggesting near-zero release from the beads initially. Considering the correlation coefficient (r) values of the zero-order and Korsmeyer–Peppas release models, both models describe the dissolution data reasonably well. Where there are competing models (with similar r values), residual analysis can be used to distinguish between the models [32]. Fig. 3B is the residual plot for the optimized formulation. The residuals are high for the zero-order, first-order, Higuchi, and Hixson–Crowell models (and least for the Korsmeyer–Peppas model, which also shows systematic deviation): the

Table 6
Comparison of responses between predicted and experimental values for the cross-validation set

Responses	Test	Factors/levels			Experimental values	Predicted values	% Relative error
		A	*B*	*C*			
% Entrapment	1	−1	−0.6	−0.6	63.26	62.50	1.2
	2	−0.6	0	0.4	65.34	63.70	2.5
	3	−0.4	0.6	0	66.23	68.08	−2.8
	4	0	−0.4	0.6	73.71	71.79	2.6
	5	0.4	0.4	−0.4	76.44	78.28	−2.4
T_{50}	1	−1	−0.6	−0.6	19.88	20.44	−2.8
	2	−0.6	0	0.4	30.28	31.10	−2.7
	3	−0.4	0.6	0	34.76	33.68	3.1
	4	0	−0.4	0.6	33.82	34.66	−2.5
	5	0.4	0.4	−0.4	38.44	37.96	1.2
T_{90}	1	−1	−0.6	−0.6	29.48	29.22	0.9
	2	−0.6	0	0.4	41.51	42.39	−2.1
	3	−0.4	0.6	0	46.83	46.09	1.6
	4	0	−0.4	0.6	45.57	46.66	−2.4
	5	0.4	0.4	−0.4	50.81	51.37	−1.1
Particle size	1	−1	−0.6	−0.6	1.75	1.71	2.1
	2	−0.6	0	0.4	1.73	1.76	−1.8
	3	−0.4	0.6	0	1.76	1.74	1.3
	4	0	−0.4	0.6	1.94	1.98	−2.2
	5	0.4	0.4	−0.4	2.03	2.06	−1.6

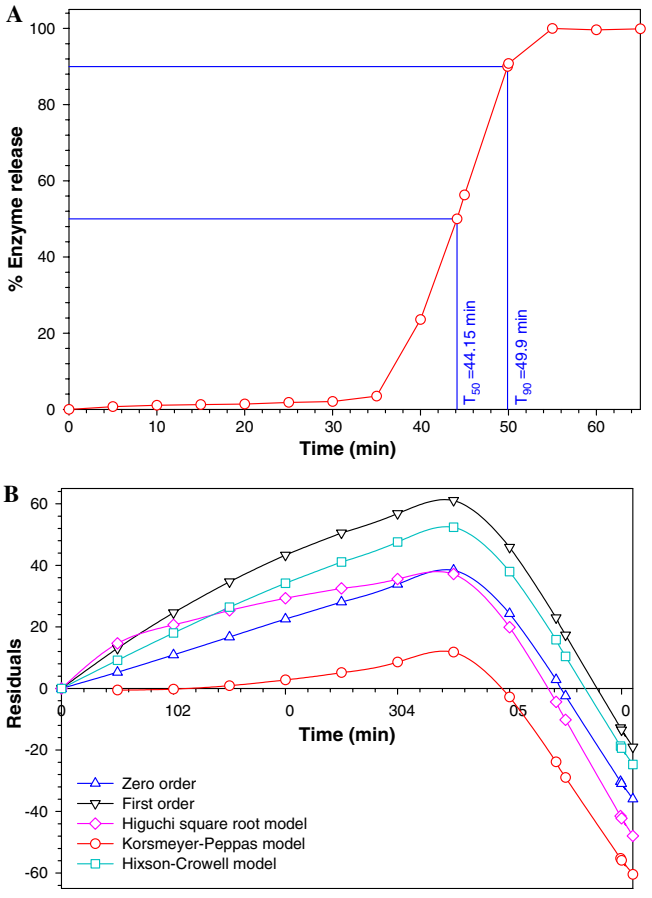

Fig. 3. (A) 'In vitro' release profile of optimized formulation (experiment 12) in SGF without enzyme pH 1.2 (USP XXVI) at 37 ± 0.5 °C. (B) Residual plot for different release models (experiment 12).

models overpredict initially and underpredict at the later stages of the dissolution process. This indicates that Korsmeyer–Peppas' power law is the best-fit model in describing the dissolution behavior of α-amylase from the chitosan–alginate PEC.

Finally, in order to determine whether the enzyme release was due to erosion or diffusion, the release data of the optimized formulation were fitted to the Kopcha model (Eq. (7)), and parameters like *A* and *B* were determined at different time intervals. As can be seen in Fig. 4A, both the diffusion and erosion terms, *A* and *B*, respectively, were almost constantly close to zero for up to 35 min. This suggests that there was neither diffusion nor erosion for the initial 35 min. The dissolution medium diffuses into the PEC in this time interval to hydrate and swell it. The erosion term, *B*, increased linearly after 35 min, indicating the predominance of erosion relative to diffusion. The hydration (the rate of which depends on the cross-linkage density, chitosan and alginate concentrations, hardening time, degree of deacetylation of chitosan, molecular masses of chitosan and alginate, pH, presence of salt counterions, etc.) was found to be the rate-limiting step for erosion initially and explains the biphasic nature of the release profile: an initial plateau followed by a steep rise in the erosion rate. This rise indicates bursting of the PEC membrane, which can be explained as follows.

When a dry hydrogel begins to absorb water, the first water molecules entering the matrix will hydrate the most polar, hydrophilic groups. As the polar groups are hydrated, the network swells and exposes hydrophobic groups, which also interact with water molecules. After the polar and hydrophobic sites have interacted with and bound

Table 7
Comparison of different dissolution kinetics models

ES[a]	Release model										
	Zero-order		First-order		Higuchi matrix		Korsmeyer-Peppas			Hixson-Crowell	
	K_0	r_0	K_1	r_1	K_H	r_H	n	K_k	r_k	K_s	r_s
19	1.88	0.80	−0.06	0.61	9.03	0.66	2.37	0.01	0.86	−0.01	0.70
11	1.62	0.80	−0.05	0.61	8.22	0.65	2.28	0.01	0.88	−0.01	0.70
24	1.46	0.81	−0.04	0.59	7.82	0.65	2.08	0.02	0.85	−0.01	0.70
31	1.59	0.81	−0.04	0.68	8.43	0.66	2.32	0.01	0.84	−0.01	0.74
23	1.42	0.81	−0.04	0.67	7.88	0.65	2.31	0.01	0.87	−0.01	0.74
20	1.17	0.78	−0.03	0.67	6.57	0.62	2.11	0.01	0.85	−0.01	0.71
7	1.30	0.78	−0.04	0.57	7.19	0.62	2.33	0.00	0.82	−0.01	0.69
16	1.06	0.75	−0.02	0.67	5.90	0.60	2.33	0.00	0.84	−0.01	0.70
4	0.96	0.75	−0.02	0.66	5.60	0.60	2.20	0.00	0.85	0.00	0.70
29	1.98	0.83	−0.05	0.72	9.48	0.68	2.49	0.01	0.90	−0.01	0.77
5	1.73	0.82	−0.06	0.57	8.79	0.67	2.34	0.01	0.89	−0.01	0.71
17	1.47	0.79	−0.03	0.70	7.49	0.64	2.15	0.01	0.85	−0.01	0.73
25	1.60	0.79	−0.04	0.63	8.10	0.64	2.37	0.01	0.86	−0.01	0.70
10	1.41	0.79	−0.04	0.62	7.53	0.64	2.21	0.01	0.87	−0.01	0.70
6	1.31	0.79	−0.04	0.56	7.29	0.64	2.17	0.01	0.87	−0.01	0.69
13	1.29	0.76	−0.03	0.66	6.85	0.61	2.38	0.00	0.84	−0.01	0.70
27	1.13	0.76	−0.02	0.66	6.30	0.61	2.21	0.01	0.85	−0.01	0.70
1	1.06	0.75	[b]	[b]	6.16	0.60	2.19	0.01	0.85	−0.01	0.61
15	1.98	0.81	−0.04	0.72	8.97	0.67	2.72	0.00	0.93	−0.01	0.76
3	1.67	0.80	−0.03	0.71	8.06	0.65	2.40	0.01	0.89	−0.01	0.75
2	1.62	0.80	−0.04	0.65	8.20	0.65	2.37	0.01	0.87	−0.01	0.72
9	1.52	0.79	−0.03	0.69	7.39	0.63	2.46	0.01	0.89	−0.01	0.73
30	1.37	0.78	−0.03	0.69	6.98	0.63	2.27	0.01	0.87	−0.01	0.72
14	1.29	0.77	−0.03	0.67	6.90	0.62	2.29	0.01	0.87	−0.01	0.71
28	1.41	0.78	−0.04	0.62	7.47	0.63	2.43	0.00	0.87	−0.01	0.70
8	1.14	0.75	−0.02	0.67	6.10	0.60	2.28	0.01	0.85	−0.01	0.70
12	**1.07**	**0.74**	**−0.02**	**0.65**	**5.94**	**0.59**	**2.21**	**0.01**	**0.83**	**−0.01**	**0.68**

[a] ES, experimental sequence.
[b] Not possible.

water molecules, the network imbibes additional water due to the osmotic driving force of the network chains toward infinite dilution. This additional swelling is opposed by the physical cross-links, leading to an elastic network retraction force. As the network swells, the network chains or cross-links begin to disintegrate at a rate depending on its composition, rate of solvent intake, and equilibrium between the osmotic pressure and the mechanical forces in the PEC membrane [40].

3.7. Characterization of optimal formulation

3.7.1. Effect of pH on release profile

The effect of the pH value on the release of α-amylase from chitosan–alginate beads in different (pH 1.2, 4.0, 6.8, and 7.4) buffers simulating the human gastrointestinal tract is shown in Fig. 4B. As with ionically cross-linked hydrogels, PEC exhibits pH-sensitive swelling under acidic conditions [22]. As the pH value changes, the charge balance inside the gel and therefore the degree of interaction between the two polymers are modified, and swelling occurs because of the dissociation of the complex. In an acidic medium, the polyacid (carboxylate, $–COO^-$, of alginate) is neutralized, and due to the free ammonium ($–NH_3^+$) groups of chitosan, free positive charges appear inside the bead. Their mutual repulsion and the entry of water together with counterions neutralizing these charges cause swelling. According to Cárdenas et al., under acidic conditions, a chitosan–alginate PEC reaches a degree of swelling five times greater than in neutral conditions [41]. Similar results were obtained in the present study and can be explained by the schematic presentation of the ionic interactions between chitosan and alginate shown in Fig. 5. As can be seen in Fig. 5A, at pH 2.0, the ionic interaction between chitosan and alginate is greatly reduced, and there is a folding of alginate with increased micropore size, which allows the greater part of the dissolution media to enter with counterions. However, at pH 6.8, the chitosan is still protonated (Fig. 5B) and forms a much stronger network with alginate with a small micropore size that restricts the entry of larger counterions. Moreover, the osmotic pressure and electrostatic repulsion responsible for swelling are balanced by the contractile force of the network, which depends on the elasticity [19] and determines the maximum degree of swelling. If the pH value is such that the global charge density of one of the polymers is no longer sufficiently high to ensure complexation, the swelling becomes very significant, and dissolution of the complex may be observed [42]. The burst effect for the optimized formulation in SGF without enzyme can thus be explained by the

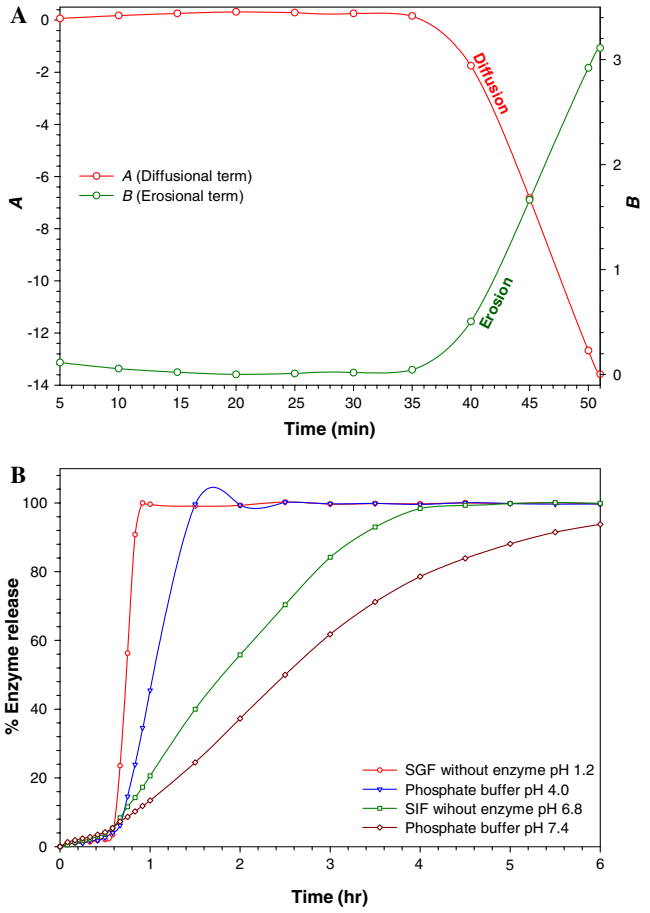

Fig. 4. (A) Kopcha model parameters (*A* and *B*) versus time profile for optimized batch (experiment 12) in SGF without enzyme pH 1.2 (USP XXVI) at 37 ± 0.5 °C. (B) Effect of pH on release profile of α-amylase entrapped in chitosan–alginate beads.

rapid swelling and lack of significant ionic interaction between the chitosan and alginate at pH 1.2. As the pH increases up to neutral, the swelling tends to decrease due to a progressively increasing number of carboxylate ($-COO^-$) groups, which interact strongly with the ammonium ($-NH_3^+$), protonated up to pH 6.8) group of chitosan. Further, the solubility of chitosan decreases at higher pH values, and it acts as a sustained-release matrix. Thus, the release of α-amylase is delayed at higher pH values.

3.7.2. FTIR spectroscopy

FTIR spectra of chitosan, sodium alginate, chitosan–alginate blank beads, α-amylase-loaded chitosan–alginate beads, a physical mixture of α-amylase and blank beads (in the same ratio as that of the optimized batch), and α-amylase are shown in Fig. 6. The FTIR spectrum of chitosan showed a weak band of C–H stretching at 2875 cm^{-1}, the absorption band of the carbonyl (C = O) stretching of the secondary amide (amide I band) at 1655 cm^{-1}, the bending vibration band of the N–H of non-acylated 2-aminoglucose primary amines at 1570 cm^{-1}, and the bending vibrations of the N–H (*N*-acetylated residues, amide II band) at 1558 cm^{-1} [43]. The peaks at 1419 and 1321 cm^{-1} belong to the N–H stretching of the amide and ether bonds and N–H stretching (amide III band), respectively. The bridge oxygen (C–O–C, cyclic ether) stretching bands at 1151, 1070, 1031, and 893 cm^{-1} were observed as well [44]. Sodium alginate showed the following distinct peaks: as a carboxyl salt it showed strong absorption bands at 1601 and 1407 cm^{-1} due to carboxyl anions (asymmetric and symmetric stretching vibrations). The α-amylase also showed various distinct peaks: one predominant band at 3380–3190 cm^{-1} (strong, s) due to the N–H stretching of secondary N-substituted amides; peaks at 2931 cm^{-1} (s) and 2898 cm^{-1} (s) due to aliphatic C–H stretching; and a strong peak at 1661 cm^{-1} due to C = O stretching of the carboxyl anion and amide group – medium bands at 1600–1500 cm^{-1} due to the C–C of the aromatic residue were also seen. Further, strong peaks between 1200 and 1050 cm^{-1} due to C–S stretching of sulfides and disulfides were observed.

For the chitosan–alginate blank beads, the band around 3500–3100 cm^{-1} becomes broader, which indicates hydrogen bonding is enhanced [45]. Moreover, the N–H bending vibration of non-acylated 2-aminoglucose primary amines (band at 1570 cm^{-1}) and asymmetric and symmetric –C–O stretching at 1601 and 1407 cm^{-1}, respectively, disappeared, indicating that the ($-NH_3^+$) of the chitosan has reacted with the $-COO^-$ of the alginate. The distinct peaks corresponding to the alginate are absent. This is probably due to the very low alginate concentration compared with chitosan and the presence of alginate at the interface. Some peaks disappeared or became weak due to interaction between or superposition of the groups of chitosan and alginate. One reason is that more chitosan was contained within the beads, and another may be that there were multi-interactions (hydrogen binding and electrostatic interaction) among the chitosan and alginate. With the incorporation of α-amylase, the spectrum of beads was similar to that of the chitosan–alginate blank beads, except for a shift at specific wavelengths. The shift can be envisaged in the difference spectrum of the blank and optimized beads, which was obtained by using the blank bead sample as a reference. The shifts in the wavelength at around 2930 cm^{-1} (C–H stretching), 1650 cm^{-1} (C = O stretching of secondary amide), 1550 cm^{-1} (N–H bending of primary amines) and 1080 cm^{-1} (C–O–C stretching of cyclic ether) may be explained through the interaction of α-amylase with chitosan. However, the physical mixture of α-amylase and blank beads showed the peaks due to both α-amylase and blank beads. This confirms amylase entrapment in the chitosan–alginate beads at the molecular level.

3.7.3. DSC

The DSC thermograms of α-amylase, chitosan, sodium alginate, the physical mixture of chitosan and alginate, the chitosan–alginate blank beads, the α-amylase-loaded optimized batch, and the physical mixture of α-amylase and blank beads are shown in Fig. 7. α-Amylase exhibited three endothermic peaks at 148.5, 215.5, and 226.8 °C,

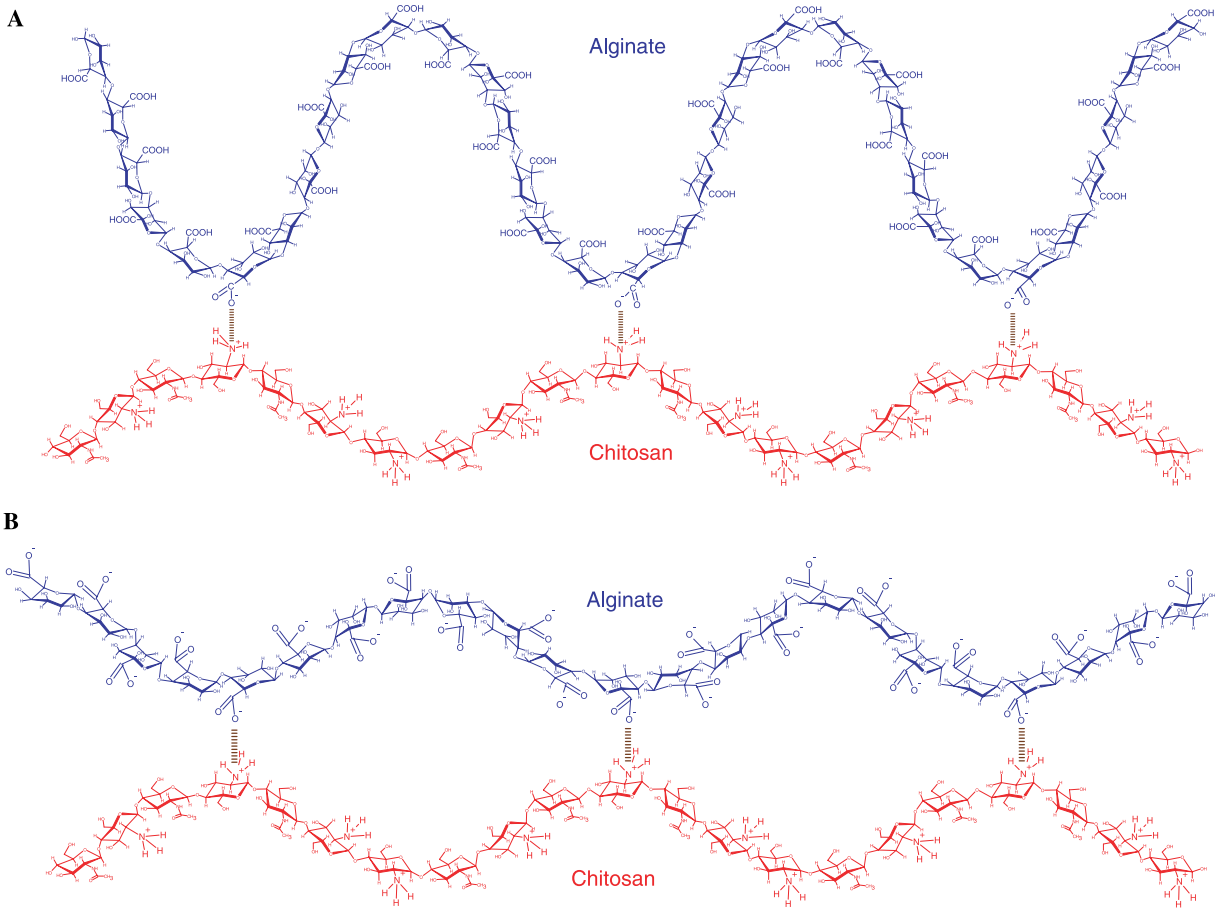

Fig. 5. Schematic representation of the ionic interactions between alginate and chitosan at (A) pH 2.0 and (B) pH 6.8.

followed by a broad degradation exotherm at 358 °C. The thermogram of the chitosan polymer exhibited an endothermic peak at about 94 °C that has been attributed to the evaporation of absorbed water. The exothermic baseline deviation beginning around 250 °C indicates the onset of chitosan degradation [46,47]. A broad endothermic peak at 87 °C in the thermogram of sodium alginate was similarly attributed to the presence of water molecules in the sample. It also showed two exothermic peaks at 251.2 and 265.5 °C. The chitosan–alginate reaction can be characterized by the disappearance of the degradation exothermic peaks of chitosan at 317.5 °C and of alginate at 251.2 °C. However, the exothermic peak at 266 °C corresponding to alginate was observed in the thermogram of the PEC. Analysis of the DSC curve for the chitosan–alginate beads showed a pair of exothermic and endothermic peaks at about 230 and 239.8 °C, respectively. The peak at 230 °C is probably related to the breakdown of weak unspecific electrostatic interactions. The thermogram of the chitosan–alginate physical mixture also showed the exothermic peak at around 230.2 °C and confirmed this. The DSC endothermic peak at around 239.8 °C, which was not observed in the thermograms of chitosan or alginate, could be assigned to the formation of an ionic pair between the carboxylate group ($-COO^-$) of alginate and the ammonium group ($-NH_3^+$) of chitosan due to dehydration during the DSC scan [48,49]. The DSC thermogram of the enzyme-loaded beads was similar to that of the blank beads, except that all the corresponding peaks were shifted to a lower temperature, which might be due to the electrostatic interaction between the α-amylase and biopolymers. However, there was no peak analogous to α-amylase. Moreover, the physical mixture of α-amylase and blank beads (in the same ratio as that of the optimized batch) showed the endothermic peak at 148.6 °C corresponding to α-amylase and other peaks (230, 239.8, and 266 °C) corresponding to blank beads. This confirms that most of the enzyme was uniformly dispersed at the molecular level in the beads.

3.7.4. Morphology of the beads

The spherical shape of the beads in the wet state was usually lost after drying, especially for beads prepared with low chitosan concentrations. With an increase in chitosan concentration, the shape of the beads was retained considerably. However, the shape of the optimized beads (experiment 12) changed to spherical disks with a collapsed center (Fig. 8) during the drying process. The beads prepared with 1.5% w/v chitosan showed a much deeper collapsed center or in some cases more than one collapsed center. The tendency to develop a collapsed center may be because of mass- and heat-transfer phenomena and/or aggregation

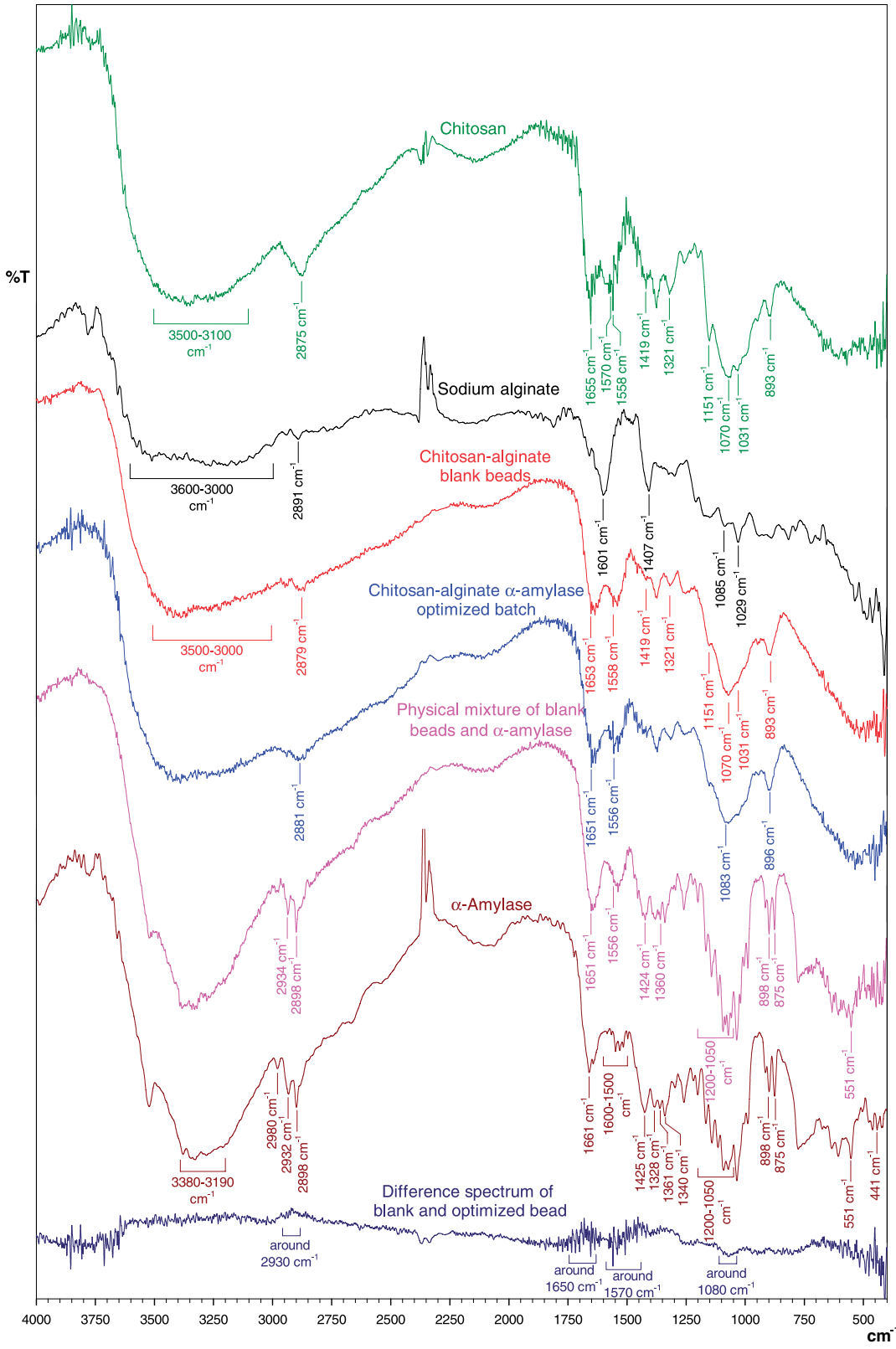

Fig. 6. The FTIR spectra of chitosan, sodium alginate, chitosan–alginate blank beads, α-amylase loaded optimized beads, physical mixture (in the ratio same as that of the optimized batch) of α-amylase and blank beads, α-amylase and difference spectrum of blank and optimized bead.

of chitosan helical fibers into bundles and the squeezing out of some water from the gel [50]. Further, a close scrutiny of Figs. 9A–C reveals the presence of fractures on the surface of the beads, developed during the drying process, through which the dissolution media enter first. The very fine mesh-like structure observed in Fig. 9D was due to a polyelectro-

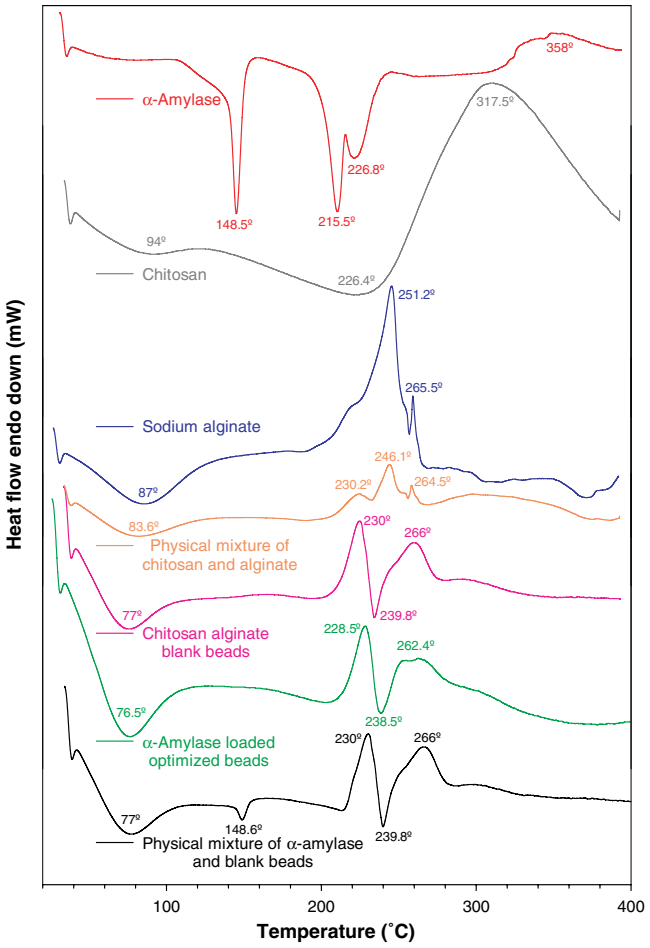

Fig. 7. The DSC thermograms of α-amylase, chitosan, sodium alginate, physical mixture of chitosan and alginate, chitosan–alginate blank beads, α-amylase loaded optimized beads, and physical mixture of α-amylase and blank beads made at the same analytical conditions.

lyte reaction and is quite comparable with many other PEC micrographs [51,52].

3.8. Stability study

For the developed formulation, the similarity factor (f_2) was calculated through a comparison of the dissolution profile at each storage condition with the control at the initial condition. The f_2 factors obtained ranged from 78 to 98, with a 2–4% average difference. Evaluation of the shelf-life was carried out as per ICH Q1E Step 4 (Evaluation of Stability Data) guidelines for drug substances intended for room temperature storage. The long-term and accelerated stability data showed little change over time, and so a shelf-life up to twice the length of the period for which long-term data are available (i.e., 24 months) can be proposed. Extrapolation of the shelf-life beyond the length of available long-term data can be proposed. For this, an approach to analyzing the data on a quantitative attribute that is expected to change with time is to determine the time at which the 95% one-sided confidence limit for the mean curve intersects the acceptance criterion (not more than 5% change on assay from its initial value) can be accepted. The long-term stability data of the developed formulation, the marketed formulation, and the bulk α-amylase were linearly extrapolated (zero-order kinetics) to calculate the shelf-life of each of these (Fig. 10), which were found be 3.68 years, 0.99 years, and 0.41 years, respectively. Hence, the stability of the entrapped α-amylase was significantly improved, compared with the conventional dosage forms.

Dumitriu and Chornet observed that hydrogels, formed through the interaction of a polycation with a protein (α-amylase in this case), have the advantage of creating an

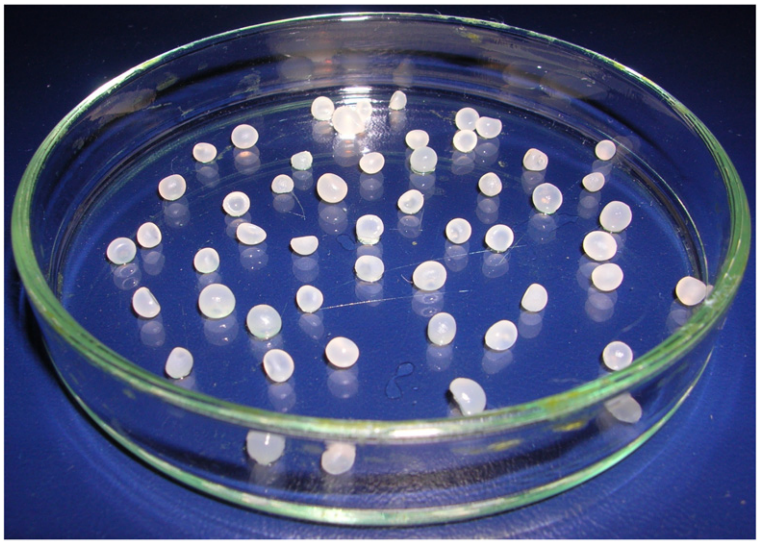

Fig. 8. Photograph of wet chitosan–alginate beads showing spherical disk shape with collapsed center during drying process.

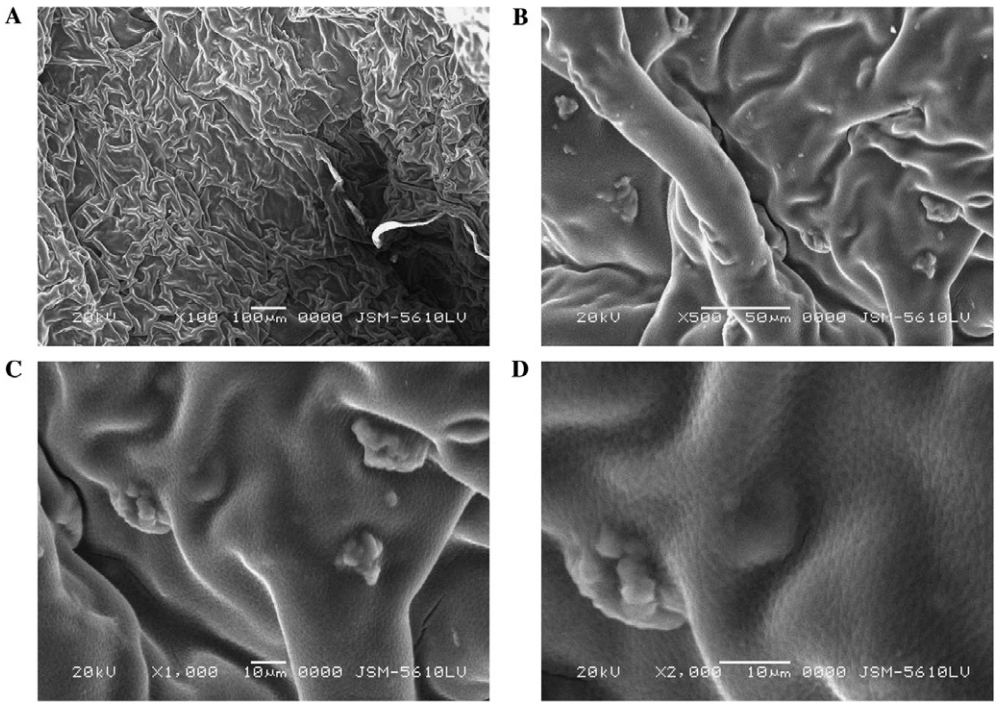

Fig. 9. SEM micrographs and surface morphology of optimized chitosan–alginate beads (formulation 12) at different magnification.

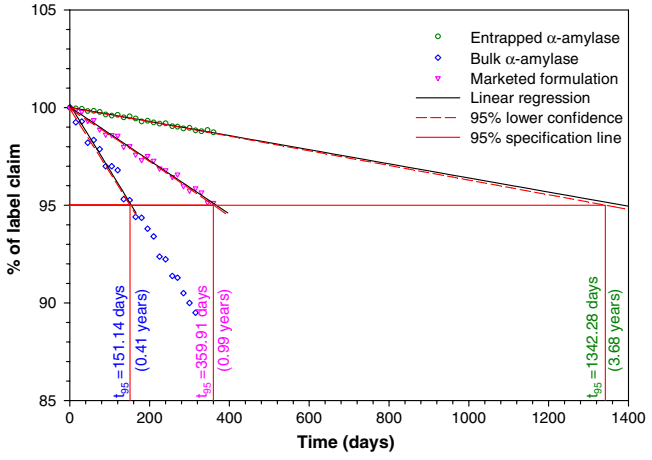

Fig. 10. Extrapolation of long-term stability data for shelf-life calculation.

ionic microsystem that favors the stabilization of a protein polymer (i.e., enzyme) by interacting with the free acid and base functions [53]. Moreover, protein–polyelectrolyte complexes also have the ability to improve the operational stability of the enzyme activity during catalysis [53]. This may be the reason for the improved stability of the α-amylase entrapped in the chitosan–alginate PEC beads.

4. Conclusions

Reversed chitosan–alginate PEC beads exhibited a promising improvement in stability of entrapped α-amylase and can find a place in the design of multiparticulate drug delivery systems. Optimization of the process using response surfaces resulted in >90% entrapment and a >48 min T_{90} value (experiment 12). The T_{50} and T_{90} values were increased with an increase in alginate concentration and hardening time, while they decreased with an increase in chitosan concentration. The percentage of entrapment was found to be directly proportional to the chitosan concentration and the alginate concentration, while it was inversely proportional to the hardening time. Mathematical analysis of the different drug release modalities and Kopcha's model revealed that after 35 min the enzyme was released due to the bursting effect. FTIR and DSC studies confirmed the entrapment of α-amylase in the chitosan–alginate beads. Texture analysis revealed a mesh-like fine structure due to the PEC reaction in the absence of added salt. Accelerated and long-term stability studies illustrated a considerably improved shelf-life of α-amylase entrapped in chitosan–alginate beads compared with the conventional dosage form. The results of the present study seem to be of value for pharmaceutical industries associated with digestive enzyme formulations, and the reversed chitosan–alginate PEC can be used for a number of applications because of the short time of reaction, simplicity, and reactivity under salt-free conditions.

Acknowledgments

We acknowledge the University Grants Commission (New Delhi, India) for availing Senior Research Fellowship to Mr. Mayur G. Sankalia. We greatly appreciate the Relax Pharmaceuticals (Vadodara, India) for skillful assistance and providing FTIR testing facility in this study.

Appendix A. Supplementary data

Supplementary data associated with this article can be found, in the online version, at doi:10.1016/j.ejpb.2006.07.014.

References

[1] E. Nuernberg, W. Hamperl, Decomposition kinetics of alpha-amylase in pancreatin under thermal and mechanical stress, Acta Pharm. Technol. (1986) 182–187.

[2] H. Guzman-Maldano, O. Paredes-Lopez, Amylolytic enzymes and products derived from starch; a review, Crit. Rev. Food Nutr. 36 (1995) 373–403.

[3] S. Dumitriu, E. Chornet, Inclusion and release of proteins from polysaccharide-based polyion complexes, Adv. Drug Deliv. Rev. 31 (1998) 223–246.

[4] E.S.N. Kokufuta, H. Tanaka, I. Nakarnura, Use of polyelectrolyte complex-stabilized calcium alginate gel for entrapment of amylase, Biotechnol. Bioeng. 32 (1988) 756–759.

[5] G.F. Bickerstaff, Immobilization of enzymes and cells: some practical considerations, in: G.F. Bickerstaff (Ed.), Immobilization of Enzymes and Cells, vol. 1, Humana Press, Totowa, NJ, 1997, pp. 1–12.

[6] M.N.V. Ravi Kumar, R.A.A. Muzzarelli, C. Muzzarelli, H. Sashiwa, A.J. Domb, Chitosan chemistry and pharmaceutical perspectives, Chem. Rev. 104 (2004) 6017–6084.

[7] E. Casal, N. Corzo, F.J. Moreno, A. Olano, Selective recovery of glycosylated caseinmacropeptide with chitosan, J. Agric. Food Chem. 53 (2005) 1201–1204.

[8] A. Charlot, R. Auzély-Velty, M. Rinaudo, Specific interactions in model charged polysaccharide systems, J. Phys. Chem. B 107 (2003) 8248–8254.

[9] E.I. Rabea, M.E.-T. Badawy, C.V. Stevens, G. Smagghe, W. Steurbaut, Chitosan as antimicrobial agent: applications and mode of action, Biomaterials 4 (2003) 1457–1465.

[10] T.A. Khan, K.K. Peh, H.S. Ching, Mechanical, bioadhesive strength and biological evaluations of chitosan films for wound dressing, J. Pharm. Pharm. Sci. 3 (2000) 303–311.

[11] P. He, S.S. Davis, L. Illum, In vitro evaluation of the mucoadhesive properties of chitosan microspheres, Int. J. Pharm. 166 (1998) 75–88.

[12] H. Ueno, T. Mori, T. Fujinaga, Topical formulations and wound healing applications of chitosan, Adv. Drug Deliv. Rev. 52 (2001) 105–115.

[13] X.F. Liu, Y.L. Guan, D.Z. Yand, Z. Li, K.D. Yao, Antibacterial actins of chitosan and carboxymethylated chitosan, J. Appl. Polym. Sci. 79 (2001) 1324–1335.

[14] R.A.A. Muzzarelli, Human enzymatic activities related to the therapeutic administration of chitin derivatives, Cell Mol. Life Sci. 53 (1997) 131–140.

[15] M.G. Peter, Applications and environmental aspects of chitin and chitosan, J. Macromol. Sci. A32 (1995) 629–640.

[16] W.H. McNeely, D.J. Pettitt, in: R.L. Whistler, J.N. Bemiller (Eds.), Industrial Gums, Academic Press, New York, 1973.

[17] Z. He, K. Wang, Alginate-konjac glucomannan-chitosan beads as controlled release matrix, Int. J. Pharm. 244 (2002) 117–126.

[18] P.G. Park, W.S.W. Shalaby, H. Park, Physical Gels, Biodegradable Hydrogels for Drug Delivery, Technomic Publishing Compony, Inc. (now CRC Press), Lancaster, PA, 1993, pp. 99–140.

[19] T. Sakiyama, H. Takata, M. Kikuchi, K. Nakanishi, Polyelectrolyte complex gel with high pH-sensitivity prepared from dextran sulfate and chitosan, J. Appl. Polym. Sci. 73 (1999) 2227–2233.

[20] K.D. Yao, H. Tu, F. Cheng, J.W. Zhang, J. Liu, pH-sensetivity of the swelling of a chitosan–pectin polyelectrolyte complex, Angew Makromol. Chem. 245 (1997) 63–72.

[21] M.M. Daly, D.W. Knorr, Chitosan–alginate complex coacervate capsules: Effects of calcium choloride, plasticizersand polyelectrolytes on mechanical stability, Biotechnol. Prog. 4 (1988) 76–81.

[22] J. Berger, M. Reist, J.M. Mayer, O. Felt, R. Gurny, Structure and interactions in chitosan hydrogels formed by complexation or aggregation for biomedical applications, Eur. J. Pharm. Biopharm. 57 (2004) 35–52.

[23] E. Tsuchida, Formation of polyelectrolyte complexes and their structures, J. Macromol. Sci. Pure Appl. Chem. A31 (1994) 1–15.

[24] G.E.P. Box, J.S. Hunter, Multi-factorial designs for exploring response surfaces, Ann. Math. Stat. 28 (1957) 195–241.

[25] R.L. Plackett, J.P. Burman, The design of optimum multifactorial experiments, Biometrika 33 (1946) 305–325.

[26] M. Gibaldi, S. Feldman, Establishment of sink conditions in dissolution rate determinations – theoretical considerations and application to non-disintegrating dosage forms, J. Pharm. Sci. 56 (1967) 1238–1242.

[27] J.G. Wagner, Interpretation of percent dissolved-time plots derived from in vitro testing of conventional tablets and capsules, J. Pharm. Sci. 58 (1969) 1253–1257.

[28] T. Higuchi, Mechanism of sustained-action medication. Theoretical analysis of rate of release of solid drugs dispersed in solid matrices, J. Pharm. Sci. 52 (1963) 1145–1149.

[29] R.W. Korsmeyer, R. Gurny, E.M. Doelker, P. Buri, N.A. Peppas, Mecanism of solute release from porous hydrophilic polymers, Int. J. Pharm. 15 (1983) 25–35.

[30] N.A. Peppas, Analysis of Fickian and non-Fickian drug release from polymers, Pharm. Acta Helv. 60 (1985) 110–111.

[31] A.W. Hixson, J.H. Crowell, Dependence of reaction velocity upon surface and agitation, Ind. Eng. Chem. 23 (1931) 923–931.

[32] S.I. Pather, I. Russell, J.A. Syce, S.H. Neau, Sustained release theophylline tablets by direct compression. Part 1: formulation and in vitro testing, Int. J. Pharm. 164 (1998) 1–10.

[33] P.L. Ritger, N.A. Peppas, A simple equation for description of solute release II. Fickian and anomalous release from swellable devices, J. Control. Release 5 (1987) 37–42.

[34] M. Kopcha, N. Lordi, K.J. Tojo, Evaluation of release from selected thermosoftening vehicles, J. Pharm. Pharmacol. 43 (1991) 382–387.

[35] B.W. Smith, J.H. Roe, A micromodification of the Smith and Roe method for the determination of amylase in body fluids, J. Biol. Chem. 227 (1957) 357–362.

[36] J. Hsiu, E.H. Fischer, E.A. Stein, Alpha-amylase as calcium-metalloenzymes. II. Calcium and the catalytic activity, Biochemistry 3 (1964) 61–66.

[37] E.W. Rice, Improved spectrophotometric determination of amylase with a new stable starch substrate solution, Clin. Chem. 5 (1959) 592–596.

[38] J.W. Lee, S.Y. Kim, S.S. Kim, Y.M. Lee, K.M. Lee, S.J. Kim, Synthesis and characteristics of interpenetrating polymer network hydrogel composed of chitosan and poly (acrylic acid), J. Appl. Polym. Sci. 73 (1999) 113–120.

[39] C.S. Brazel, N.A. Peppas, Mechanisms of solute and drug transport in relaxing, swellable, hydrophilic glassy polymers, Polymers 40 (1999) 3383–3398.

[40] A.S. Hoffman, Hydrogels for biomedical applications, Adv. Drug Deliv. Rev. 43 (2002) 3–12.

[41] A. Cárdenas, W. Argüelles-Monal, F.M. Goycoolea, I. Higuera-Ciapara, C. Peniche, Diffusion through membranes of the polyelectrolyte complex of chitosan and alginate, Macromol. Biosci. 3 (2003) 535–539.

[42] V. Chavasit, C.A. Kienzle-Sterzer, J.A. Torres, Formation and characterization of an insoluble polyelectrolyte complex: chitosan–polyacrylic acid, Polym. Bull. 19 (1988) 223–230.

[43] C. Le-Tien, M. Millette, M.-A. Mateescu, M. Lacroix, Modified alginate and chitosan for lactic acid bacteria immobilization, Biotechnol. Appl. Biochem. 39 (2004) 347–354.

[44] E. Khor, The structural properties of chitin as it is known today, Chitin: Fulfilling a Biomaterials Promise, Elsevier, New York, 2001, pp. 73–82.
[45] J.H. Yu, Y.M. Du, H. Zheng, Blend films of chitosan–gelation, J. Wuhan Univ. (Nal. Sci. Ed.) 45 (1999) 440–444.
[46] M.N. Khalid, F. Agnely, N. Yagoui, J.L. Grossiord, G. Couarraze, Water sate characterization, swelling behavior, thermal and mechanical properties of chitosan based networks, Eur. J. Pharm. Sci. 15 (2002) 425–432.
[47] O. Borges, G. Borchard, J.C. Verhoef, A.d. Sousa, H.E. Junginger, Preparation of coated nanoparticles for a new mucosal vaccine delivery system, Int. J. Pharm. 299 (2005) 155–166.
[48] L. Wang, E. Khor, L.Y. Lim, Chitosan–alginate-$CaCl_2$ system for membrane coat application, J. Pharm. Sci. 90 (2001) 1134–1142.
[49] C. Tapia, E. Costa, M. Moris, J. Sapag-Hagar, F. Valenzuela, C. Basualto, Study of the influence of the pH media dissolution, degree of polymerization, and degree of swelling of the polymers on the mechanism of release of diltiazem from matrices based on mixtures of chitosan/alginate, Drug Dev. Ind. Pharm. 28 (2002) 217–224.
[50] J.L. Iborra, A. Manjon, M. Canovas, Immobilization in carrageenans, in: G.F. Bickerstaff (Ed.), Immobilization of Enzymes and Cells, vol. 1, Humana Press, Totowa, New Jersey, 1997, pp. 53–60.
[51] J.S. Lee, D.S. Cha, H.J. Park, Survival of freeze-dried Lacrobacillus bulgaricus KFRI 673 in chitosan-coated calcium alginate microparticles, J. Agric. Food Chem. 52 (2004) 7300–7305.
[52] M.C.P. Cruz, S.P. Ravagnani, F.M.S. Brogna, S.P. Campana, G.C. Triviño, A.C. Luz Lisboa, L.H.I. Mei, Evaluation of the diffusion coefficient for controlled release of oxytetracycline from alginate/chitosan/poly(ethylene glycol) microbeads in simulated gastrointestinal environments, Biotechnol. Appl. Biochem. 40 (2004) 243–253.
[53] D. Severian, C. Esteban, Inclusion and release of proteins from polysaccharide-based polyion complexs, Adv. Drug Deliv. Rev. 31 (1998) 223–246.